Structure and Morphology of Poly(lactic acid) Stereocomplex Nanofiber Shish Kebabs

Qing Xie[1,2,#], Xiaohua Chang[1,2,#], Qian Qian[2], Pengju Pan[1,*], Christopher Y. Li[2,*]

[1] State Key Laboratory of Chemical Engineering, College of Chemical and Biological Engineering, Zhejiang University, 38 Zheda Road, Hangzhou 310027, China

[2] Department of Materials Science and Engineering, Drexel University, Philadelphia, PA 19104, USA

[#] equal contribution

[*] Correspondence authors: chrisli@drexel.edu, panpengju@zju.edu.cn

KEYWORDS: poly(lactic acid), polymer crystallization, polymer single crystals, stereocomplex, nanofiber shish kebab

ABSTRACT: We report the formation and structure of poly(lactic acid) (PLA) nanofiber shish kebabs (NFSKs) containing stereocomplex crystal (SC) shish and SC/homocrystal (HC) kebabs. PLA-based NFSKs were obtained by combining electrospinning and controlled polymer crystallization in order to investigate the interplay between PLA SC and HC formation. Nanofibers were produced by electrospinning poly(L-lactic acid)/poly(D-lactic acid) (PLLA/PDLA) blends and were used as the shish. A secondary polymer (either PDLA or PLLA/PDLA blends) was decorated on the nanofiber by an incubation method to form kebab lamellae. We show that both SC and HC kebab crystals can be formed using a SC shish following a soft epitaxy mechanism, while the subtle morphological differences in the resultant NFSKs reveal the propensity of SC nuclei in SC/HC crystallization.

Polymer nanofibers have found broad applications in various research fields.[1-3] With the development of numerous novel electrospinning techniques, great successes have been achieved in controlling nanofiber surface morphology and structure.[1-3] In particular, hierarchically ordered nanofibers can be fabricated by combining electrospinning and controlled polymer crystallization techniques.[4] Electrospun nanofibers serve as 1D nucleating agents which induce the crystallization of a secondary polymer, leading to a unique morphology mimicking the classical shish kebab polymer crystals obtained in flow-induced crystallization[5, 6] and the nano hybrid shish kebab structure observed in carbon nanotube-induced polymer crystallization.[7-9] This intriguing morphology was named as *nanofiber shish kebab* (NFSK), as the preformed nanofiber serve as the shish nuclei. Previous work showed the feasibility of forming polycaprolactone and poly(ethylene oxide) NFSKs.[4, 10, 11] The shish kebab structure provides a new means to assemble nanoparticles,[12] control biomineralization,[11] and guide cell growth.[13-15] For biomedical and biomineralization applications, poly(lactic acid) (PLA) has been extensively studied since it is biocompatible and biodegradable. Compared to poly(L-lactic acid) (PLLA) and poly(D-lactic acid) (PDLA) homocrystals (HCs), because of the intermolecular H-bonding, polymer chains pack more closely in the crystalline lattice of PLA stereocomplex crystals (SC),[16-18] leading to enhanced properties of PLA SCs such as high melting temperature (T_m)[19], good thermal resistance[18], mechanical properties[20], and solvent resistance.[21]

The formation of HCs and SCs are often kinetically entangled in PLLA/PDLA blends crystallization. While HCs and SCs compete for feeding polymers, SCs can also act as the nucleating agent for the crystallization of enantiomeric PLA[22, 23] or PLLA/PDLA blends[24] in bulk crystallization. The interplay of HCs and SCs has been studied in bulk systems using thermal analysis techniques, yet it is unclear how, on the molecular or single crystal level, the two types of dramatically different crystals morphologically and structurally interact. In this work, we approach this problem by producing PLLA/PDLA SC nanofibers and subsequently using them as the 1D nucleating agents to study the crystallization of PLA SCs as well as HCs. NFSK structures were discovered in both cases, confirming the nucleation of HC and SCs on existing SC nanofibers. The differences in NFSK morphologies also provided a structural marker for better understanding SC-induced PLA HC and SC growth.

Stereocomplex PLA nanofibers were obtained by electrospining 8 wt.% equal mass PLLA (Mw = 200 kg/mol, $Đ$ = 1.71) and PDLA (Mw = 215 kg/mol, $Đ$ = 1.65) hexafluoroisopropanol (HFIP) solution following reported methods.[25-27] The feeding rate, voltage, and collecting distance were controlled to be 1 ml/h, 15 kV, and 15 cm, respectively. Nanofibers with an average diameter of ~ 800 nm were obtained as seen from the scanning electron microscopy (SEM) image in Figure 1a. Differential scanning calorimetry (DSC) and wide-angle X-ray diffraction (WAXD) experiments confirmed the formation of PLA SCs (see later discussion). The as-formed nanofibers were then

used as the 1D templates for PLA crystallization study. For a typical crystallization process, 0.03 wt.% PLLA (Mw = 10 kg/mol, $Đ \leq 1.10$) and PDLA (Mw = 13.6 kg/mol, $Đ \leq 1.10$) were dissolved separately in *p*-xylene at 130 °C for 1h, mixed and then slowly cooled to a pre-determined crystallization temperature (T_c) in an oil bath. The SC-PLA nanofibers were incubated in the mixed solution for a certain crystallization time. Note that because of the excellent solvent resistance of PLA SCs, these nanofibers are stable in organic solvents such as *p*-xylene for at least 12h at 83 °C as the SEM images showed that the fiber morphology was intact after incubation (Figure S1). Figures 1b,c show SEM images with different magnifications of the SC nanofibers after 4h of incubation. NFSK morphology is seen, with dense polymer lamellar crystals uniformly growing orthogonal to the nanofiber axis, forming the kabab crystals. The lamellae also appear slightly wavy, which results from partial merge of multiple adjacent lamellae as pointed by the arrows in Figure 1c.

The crystalline nature of the PLA nanofibers and NFSKs was characterized by WAXD and DSC. **Figures 1d-f** are the 2-D WAXD fiber patterns and the corresponding azimuthal integration profiles. The diffraction peaks located at $q = 0.85$, 1.47, and 1.70 Å^{-1} ($d = 0.738$, 0.427, 0.369 nm) are characteristic of the (110), (300)/(030), and (220) reflections of PLA SCs, respectively.[28] In the nanofiber fiber diffraction pattern (**Figure 1d**), the (110) arcs are clearly located on the meridian, which is perpendicular to the fiber axis (equator direction), indicating that the PLLA and PDLA chains are parallel to the fiber axis. The absence of PLA HC diffraction peaks suggests that electrospinning promotes mutual diffusion and interactions between PLLA and PDLA chains in the blend nanofibers, and the polymers crystallized in the SC form. SC structures can also be seen in NFSK (**Figures 1e**) and the (110) diffraction arcs are also located on the meridian, indicating that the kabab crystals are SC and the PLA chains in the kebabs are parallel to the nanofiber axis, which confirms the soft epitaxy mechanism in the formation of NFSKs.[4, 9] Herein we use NFSK$^{\text{SC-PLA/SC-PLA}}$ to describe the NFSK morphology observed in **Figure 1**, where the first superscript SC-PLA denotes the shish polymer while the second one represents the kebab polymer. **Figure 1g** shows the DSC first heating thermograms of the SC nanofibers and NFSK$^{\text{SC-PLA/SC-PLA}}$. A single melting peak can be observed in both cases and the melting temperature is approximately 225 °C, which is associated with SC melting. No HC crystal melting was observed, which is consistent with the WAXD results. The crystallinities of SC ($X_{c,SC}$) in SC-PLA nanofibers and NFSK$^{\text{SC-PLA/SC-PLA}}$ are around 44.1% and 45.8%, respectively, which was calculated from $X_{c,SC} = \Delta H_m/\Delta H^0_{m,SC} \times 100\%$ ($\Delta H^0_m = 142$ J/g for SCs[29]). This result indicates that the crystallinity of kebabs is greater than that of the shish, which is attributed to the dramatically different formation processes of the shish and kebab crystals.

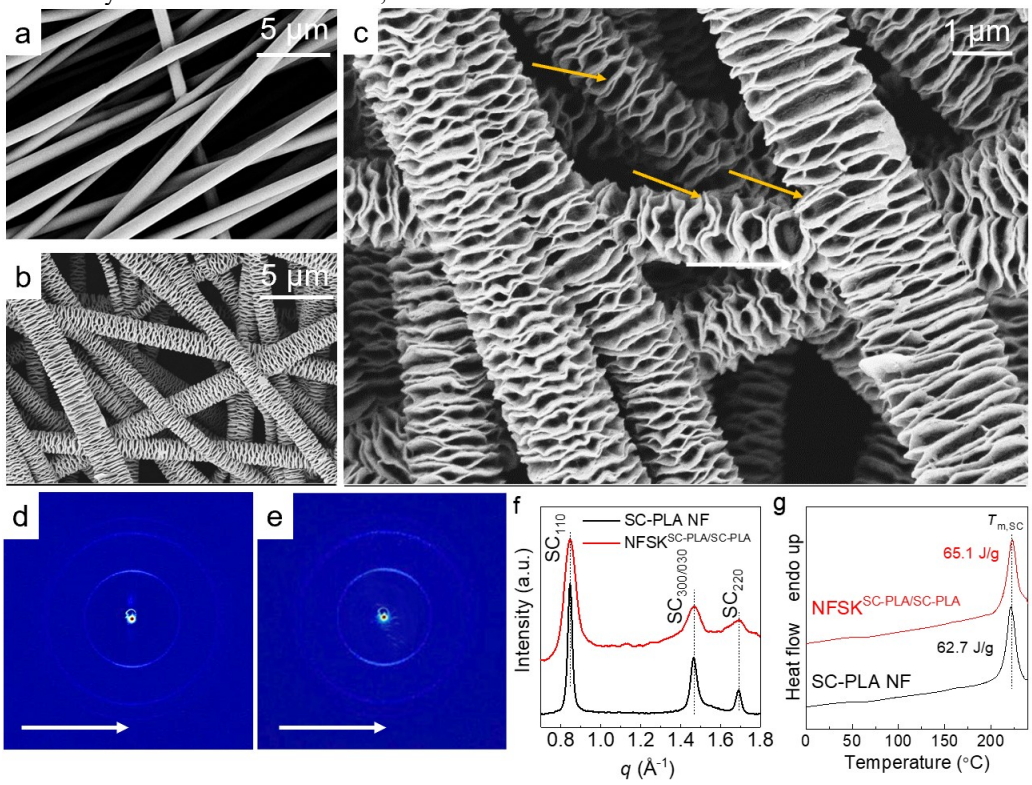

Figure 1. Morphology and structure of SC-PLA nanofiber and NFSK$^{\text{SC-PLA/SC-PLA}}$. (a-c) show SEM images of (a) SC-PLA nanofibers and (b,c) SC-PLA nanofiber incubated in 0.03wt% PLLA/PDLA/*p*-xylene for 4h. (d-e) are 2D WAXD patterns of (d) SC-PLA nanofibers and (e) NFSK$^{\text{SC-PLA/SC-PLA}}$, respectively. White arrows in the figure indicate fiber axes. (f-g) are the (f) WAXD profiles and (g) DSC heating thermograms of nanofibers and NFSKs.

To better understand how the kebab crystals form on nanofibers, temporal evolution of the crystal growth was investigated by quenching the NFSK at different time points of the growth, as shown in **Figures 2a-e**. After 10 min of incubation, small particles can be observed uniformly distributed on the fiber surface. These particles gradually become anisotropic plates aligning perpendicular to the fiber axis, indicating that the particles in **Figure 2a** are crystal nuclei formed heterogeneously on the nanofiber surface. The surface nucleation density in **Figure 2a** can be estimated to be ~ 436 sites/μm^2, which is

quite dense. These nuclei then grow perpendicularly to the fiber and develop into large pieces wrapping around the shish nanofiber, leading to the observed toroidal shaped kebab crystal in the late stage of the growth. **Figure 2f** reveals that the kebab lateral size (defined as (D-d)/2, where D and d are the diameters of NFSK and nanofiber, respectively) increases linearly with growth time from t ~ 0-5 h, with a radial growth rate of ~ 76 nm/h. After 5 h, the growth rate decreases to ~ 13 nm/h, perhaps due to the consumption of the free polymers in solution. Of interest is that the kebab period gradually increases with crystal growth as well: the kebab period is approximately ~ 70 nm at 60 min, increasing to ~ 200 nm at 120 min, and to ~ 220 nm after 15h. As the kebab crystals grow larger, due to the diffusion-limited concentration gradient at the growth front, only a fraction of the kebabs can further develop into larger size, and the observed kebab period therefore increases.

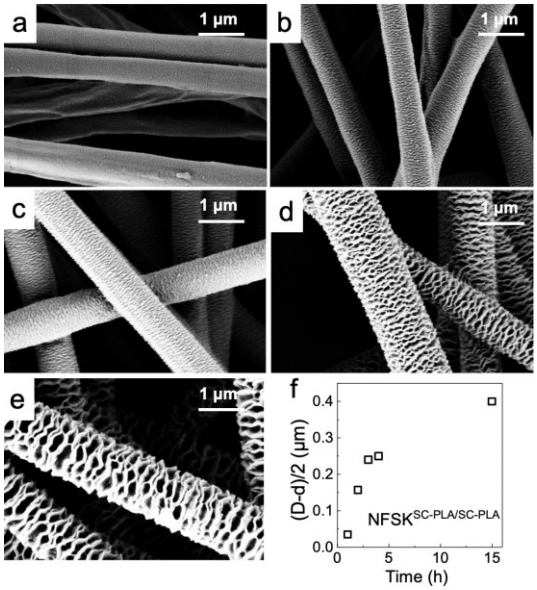

Figure 2. SEM images SC-PLA nanofibers incubated in 0.03 wt.% PLLA/PDLA/*p*-xylene for (a) 10 min, (b) 30 min, (c) 1h, (d) 2h, and (e) 3h. (f) Plot of kebab lateral size [(D-d)/2] *vs.* time.

The formation of SC-PLA nanofiber provides us a unique opportunity to study SC-PLA-induced HC crystal growth. To this end, the SC-PLA nanofibers were incubated in 0.03 wt% PDLA (13.6 kg/mol)/*p*-xylene at 80 °C and PLLA (10 kg/mol)/*p*-xylene at 70 °C, respectively. NFSK structures were observed in both cases where thin lamellar crystals were formed perpendicular to the fiber axis, as shown in **Figures 3a, b**. DSC first heating thermograms are shown in **Figure 3c**. In both cases, in addition to the previously observed SC melting peak at around 223°C, additional double melting peaks located at 159/172 °C, and 159/169 °C, can be seen for PDLA and PLLA samples, respectively, indicating the kebabs in **Figures 3a, b** are HCs. The double melting of HCs can be attributed to the melting/recrystallization/melting process during heating,[30] and the crystallinity of HC ($X_{c,HC}$) was 24.6% and 20.8% for PDLA and PLLA samples, respectively, which was calculated from $X_{c,HC} = \Delta H_m/\Delta H^0_{m,HC} \times 100\%$ ($\Delta H^0_{m,HC} = 93$ J/g for HCs[31]). The fiber morphology observed in **Figures 3a, b** can therefore be described as NFSK$^{SC\text{-}PLA/PDLA}$ and NFSK$^{SC\text{-}PLA/PLLA}$, respectively, where the superscripts PDLA and PLLA denote the kebab crystals. The crystalline structure of NFSK$^{SC\text{-}PLA/PDLA}$ and NFSK$^{SC\text{-}PLA/PLLA}$ was confirmed using WAXD, as shown in **Figure 3d**. In addition to the SC diffractions at q = 0.85, 1.47, and 1.70 Å^{-1} corresponding to (110), (300)/(030), and (220) planes of the SCs, the diffractions of α-HCs (q = 1.19 Å^{-1}, d = 0.528 nm, (110)/(200) plane of α-HCs)[32] can be observed. Diffractions of HCs and HCs can also be pbserved in the 2D WAXD patterns of NFSK$^{SC\text{-}PLA/PDLA}$ (Figure S2). The relatively large DSC melting peaks and strong XRD diffractions of HCs in Figures 3c,d imply that the HC kebabs have high crystallinity in the NFSK$^{SC\text{-}PLA/HC\text{-}PLA}$.

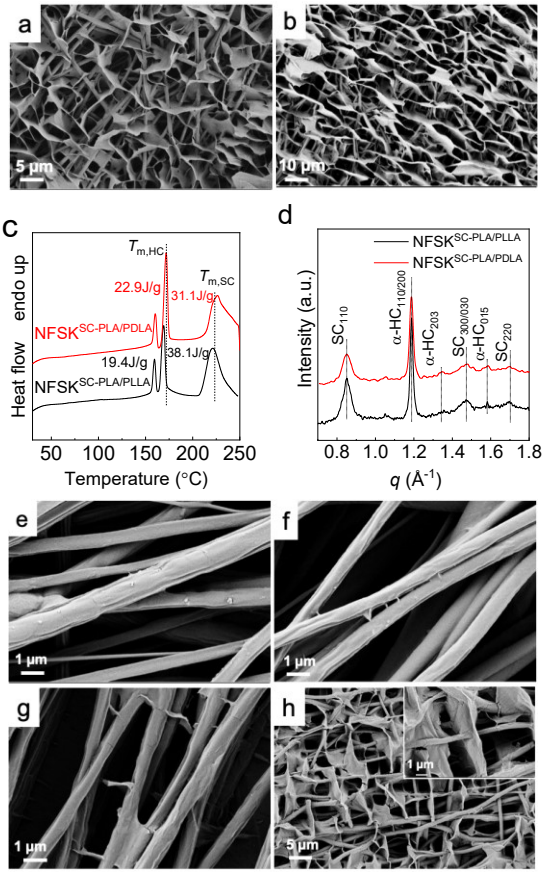

Figure 3. Morphology and structure of NFSK$^{SC\text{-}PLA/PDLA}$ and NFSK$^{SC\text{-}PLA/PLLA}$. (a-b) SEM images of (a) NFSK$^{SC\text{-}PLA/PDLA}$ and (b) NFSK$^{SC\text{-}PLA/PLLA}$ after 15 h of incubation. (c) DSC heating curves, and (d) WAXD profiles of NFSK$^{SC\text{-}PLA/PDLA}$ and NFSK$^{SC\text{-}PLA/PLLA}$. (e-h) SEM images of SC-PLA nanofibers incubated in 0.03% PDLA/*p*-xylene for (e) 10 min, (f) 30 min, (g) 2h, and (h) 8h.

The propensity of SC crystals on nucleating HC crystals can also be observed in spherulite growth as shown in Figure S3. HC spherulites are able to grow on the surface of the preformed SC spherulites. Compared with NFSK$^{SC\text{-}PLA/SC\text{-}PLA}$, kebab crystals in NFSK$^{SC\text{-}PLA/PDLA}$ and NFSK$^{SC\text{-}PLA/PLLA}$ are relatively larger with greater kebab period (3.3 μm). To better understand the formation process, temporal evolution of the HC NFSKs was studied. After 10 min incubation, few nucleation sites are formed along the nanofibers (**Figure 3e**), which is quite different from the SC case. The nucleation density is around ~0.88 sites/μm^2, significantly less than NFSK$^{SC\text{-}PLA/SC\text{-}PLA}$ (~436 sites/μm^2). After 30 min of incubation, a few small crystallites are formed along the nanofibers (**Figure 3f**). Given longer time (2h), these crystals grow larger and start to wrap the shish (**Figure 3g**) and the toroid kebab morphology start to merge after

extended incubation time. As shown in **Figure 3h**, after 8h incubation, the kebab size increases from ~400 nm to ~3.6 μm. Inset of **Figure 3h** also shows the lozenge feature of the crystal which is typical for PDLA single crystals.[33] After 15 h incubation, the kebab size further increases to ~4 μm (**Figure 3a**) with a period of ~ 3.3 μm, both are much greater than that NFSK$^{SC\text{-}PLA/SC\text{-}PLA}$ kebabs.

NFSK images in **Figures 1-3** suggest different crystallization mechanisms of SC induced SC or HC crystallization. The schematic representation of the formation mechanism of NFSK$^{SC\text{-}PLA/SC\text{-}PLA}$ and NFSK$^{SC\text{-}PLA/HC\text{-}PLA}$ is shown in **Figure 4**. During electrospinning, PLLA and PDLA chains are stretched and aligned parallel to the fiber axis, which was confirmed by the WAXD results. Free PLLA and PDLA chains from the solution then nucleate on the nanofiber surface, and the crystal growth is therefore templated by the PLA nanofibers. The orthogonal orientation of the kabab lamellae and the nanofiber axis in all NFSKs indicate that the polymer chains in the kebabs are parallel to the nanofiber axis, following the previous discussed soft epitaxy mechanism.[4, 9] The obvious differences in kebab crystal density and sizes in HC and SC NFSKs can be attributed to the differences in nucleation and growth kinetics of the HC and SC on SC-PLA nanofibers. Polymer chains adopt a 3_1 helix conformation in PLA SCs,[34] while, α-HCs of PLLA or PDLA adopts a 10_3 helix conformation,[35] which leads to a crystallographic mismatch between SC and HC crystals. Therefore, nucleation of SC on the SC-PLA nanofibers is highly efficient while PLLA/PDLA crystals nucleate much slower on the nanofiber (**Figure 4**). This explains that SC crystals were densely formed on the nanofiber surface and the period of NFSK$^{SC\text{-}PLA/SC\text{-}PLA}$ (~220 nm) is much smaller than that of NFSK$^{SC\text{-}PLA/PDLA}$ (~3.3 μm). On the other hand, due to the steric hindrance and the strong interaction of SCs, the SC crystals rarely develop into large lamellae while HC crystals can easily grow into micrometer sizes, leading to the observed small SC kebabs (~ 480 nm) and large HC ones (~ 4 μm).

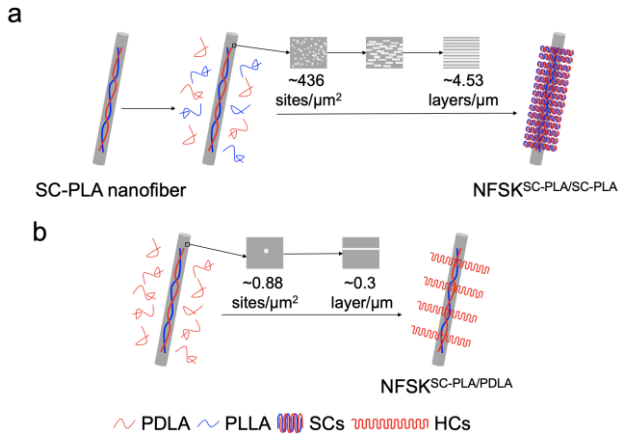

Figure 4. Schematic representation of the formation mechanism of (a) NFSK$^{SC\text{-}PLA/SC\text{-}PLA}$ and (b) NFSK$^{SC\text{-}PLA/HC\text{-}PLA}$. Note that in both cases, the polymer chains in kebab crystals are parallel to the nanofiber axis, which is defined as soft epitaxy.

In conclusion, by combining electrospinning and controlled polymer crystallization methods, hierarchically ordered PLA NFSKs were successfully obtained. In the NFSKs, the SC-PLA nanofibers served as the shish, and PLA, either in the form of HC or SC, was decorated on the SC-PLA nanofiber to form single crystal kebabs. The formation of NFSK was attributed to the soft epitaxy mechanism and confirms the capability of SC crystals in nucleating PLA SC and HC. While both SCs and HCs can be formed on the SC fiber surface, the surface nucleation density of HCs on the SC nanofibers was found to be a few hundred times lower than that of their SC counterparts, which was attributed to the crystallographic mismatching of 10_3 helix of α-HCs and 3_1 helix of SCs. The NFSK structure is of technological interest because it selectively modifies the surface of nanofibers and could introduce multifunctionalities onto the nanofibers in an ordered fashion.

ASSOCIATED CONTENT

Supporting Information

The Supporting Information is available free of charge on the ACS Publications website at DOI:

Experimental details, 2D XRD pattern, SEM and POM images.

AUTHOR INFORMATION

Corresponding Author

* E-mail: chrisli@drexel.edu
* E-mail: panpengju@zju.edu.cn

Author Contributions

#These authors contributed equally to this work.

Notes

The authors declare no competing financial interest.

ACKNOWLEDGMENT

This research was financially supported by the National Science Foundation DMR-1507760 and CMMI-1709136. Q. Xie is grateful to the financial support by the China Scholarship Council (CSC) for studying abroad. X.H. Chang is grateful to the financial support by the Zhejiang University for studying abroad.

REFERENCES

(1) Reneker, D. H.; Chun, I. Nanometre Diameter Fibres of Polymer, Produced by Electrospinning. *Nanotechnology* **1996,** *7*, 216-223.

(2) Greiner, A.; Wendorff, J. H. Electrospinning: A Fascinating Method for the Preparation of Ultrathin Fibers. *Angew. Chem. Int. Ed.* **2007,** *46*, 5670-5703.

(3) Xue, J.; Wu, T.; Dai, Y.; Xia, Y. Electrospinning and Electrospun Nanofibers: Methods, Materials, and Applications. *Chem. Rev.* **2019,** *119*, 5298-5415.

(4) Wang, B.; Li, B.; Xiong, J.; Li, C. Y. Hierarchically Ordered Polymer Nanofibers Via Electrospinning and Controlled Polymer Crystallization. *Macromolecules* **2008,** *41*, 9516-9521.

(5) Somani, R. H.; Yang, L.; Zhu, L.; Hsiao, B. S. Flow-Induced Shish-Kebab Precursor Structures in Entangled Polymer Melts. *Polymer* **2005,** *46*, 8587-8623.

(6) Cui, K.; Ma, Z.; Tian, N.; Su, F.; Liu, D.; Li, L. Multiscale and Multistep Ordering of Flow-Induced Nucleation of Polymers. *Chem. Rev.* **2018,** *118*, 1840-1886.

(7) Laird, E. D.; Li, C. Y. Structure and Morphology Control in Crystalline-Polymer/Carbon-Nanotube Composites. *Macromolecules* **2013,** *46*, 2877-2891.

(8) Li, C. Y.; Li, L.; Cai, W.; Kodjie, S. L.; Tenneti, K. K. Nanohybrid Shish-Kebabs: Periodically Functionalized Carbon Nanotubes. *Adv. Mater.* **2005,** *17*, 1198-1202.

(9) Li, L.; Li, C. Y.; Ni, C. Y. Polymer Crystallization-Driven, Periodic Patterning on Carbon Nanotubes. *J. Am. Chem. Soc.* **2006,** *128*, 1692-1699.

(10) Chen, X.; Dong, B.; Wang, B. B.; Shah, R.; Li, C. Y. Crystalline Block Copolymer Decorated, Hierarchically Ordered Polymer Nanofibers. *Macromolecules* **2010,** *43*, 9918-9927.
(11) Chen, X.; Wang, W.; Cheng, S.; Dong, B.; Li, C. Y. Mimicking Bone Nanostructure by Combining Block Copolymer Self-Assembly and 1D Crystal Nucleation. *ACS Nano* **2013,** *7*, 8251-8257.
(12) Li, B.; Li, L. Y.; Wang, B. B.; Li, C. Y. Alternating Patterns on Single-Walled Carbon Nanotubes. *Nat. Nanotech.* **2009,** *4*, 358-362.
(13) Chen, X.; Gleeson, S. E.; Yu, T.; Khan, N.; Yucha, R. W.; Marcolongo, M.; Li, C. Y. Hierarchically Ordered Polymer Nanofiber Shish Kebabs as a Bone Scaffold Material. *J. Biomed. Mater. Res. A* **2017,** *105*, 1786-1798.
(14) Yu, T.; Gleeson, S. E.; Li, C. Y.; Marcolongo, M. Electrospun Poly (ε-Caprolactone) Nanofiber Shish Kebabs Mimic Mineralized Bony Surface Features. *J. Biomed. Mater. Res. B* **2019,** *107*, 1141-1149.
(15) Attia, A. C.; Yu, T.; Gleeson, S. E.; Petrovic, M.; Li, C. Y.; Marcolongo, M. A Review of Nanofiber Shish Kebabs and Their Potential in Creating Effective Biomimetic Bone Scaffolds. *Regen. Eng. Transl. Med.* **2018,** *4*, 107-119.
(16) Tsuji, H. Poly(Lactic Acid) Stereocomplexes: A Decade of Progress. *Adv. Drug Deliv. Rev.* **2016,** *107*, 97-135.
(17) Li, Z.; Tan, B. H.; Lin, T.; He, C. Recent Advances in Stereocomplexation of Enantiomeric PLA-Based Copolymers and Applications. *Prog. Polym. Sci.* **2016,** *62*, 22-72.
(18) Bai, H.; Deng, S.; Bai, D.; Zhang, Q.; Fu, Q. Recent Advances in Processing of Stereocomplex-Type Polylactide. *Macromol. Rapid Comm.* **2017,** *38*, 1700454-1700466.
(19) Ikada, Y.; Jamshidi, K.; Tsuji, H.; Hyon, S. H. Stereocomplex Formation between Enantiomeric Poly(Lactides). *Macromolecules* **1987,** *20*, 904-906.
(20) Tsuji, H.; Ikada, Y. Stereocomplex Formation between Enantiomeric Poly(Lactic Acid)S. Xi. Mechanical Properties and Morphology of Solution-Cast Films. *Polymer* **1999,** *40*, 6699-6708.
(21) Pan, P.; Yang, J.; Shan, G.; Bao, Y.; Weng, Z.; Cao, A.; Yazawa, K.; Inoue, Y. Temperature-Variable FTIR and Solid-State ^{13}C NMR Investigations on Crystalline Structure and Molecular Dynamics of Polymorphic Poly(L-Lactide) and Poly(L-Lactide)/Poly(D-Lactide) Stereocomplex. *Macromolecules* **2012,** *45*, 189-197.
(22) Tsuji, H.; Takai, H.; Saha, S. K. Isothermal and Non-Isothermal Crystallization Behavior of Poly(L-Lactic Acid): Effects of Stereocomplex as Nucleating Agent. *Polymer* **2006,** *47*, 3826-3837.
(23) Rahman, N.; Kawai, T.; Matsuba, G.; Nishida, K.; Kanaya, T.; Watanabe, H.; Okamoto, H.; Kato, M.; Usuki, A.; Matsuda, M.; Nakajima, K.; Honma, N. Effect of Polylactide Stereocomplex on the Crystallization Behavior of Poly(L-Lactic Acid). *Macromolecules* **2009,** *42*, 4739-4745.
(24) Henmi, K.; Sato, H.; Matsuba, G.; Tsuji, H.; Nishida, K.; Kanaya, T.; Toyohara, K.; Oda, A.; Endou, K. Isothermal Crystallization Process of Poly(L-Lactic Acid)/Poly(D-Lactic Acid) Blends after Rapid Cooling from the Melt. *ACS Omega* **2016,** *1*, 476-482.
(25) Zhang, P.; Tian, R.; Na, B.; Lv, R.; Liu, Q. Intermolecular Ordering as the Precursor for Stereocomplex Formation in the Electrospun Polylactide Fibers. *Polymer* **2015,** *60*, 221-227.
(26) Lv, R.; Tian, R.; Na, B.; Zhang, P.; Liu, Q. Strong Confinement Effects on Homocrystallization by Stereocomplex Crystals in Electrospun Polylactide Fibers. *J. Phys. Chem. B* **2015,** *119*, 15530-15535.
(27) Jing, Y.; Zhang, L.; Huang, R.; Bai, D.; Bai, H.; Zhang, Q.; Fu, Q. Ultrahigh-Performance Electrospun Polylactide Membranes with Excellent Oil/Water Separation Ability Via Interfacial Stereocomplex Crystallization. *J. Mater. Chem. A* **2017,** *5*, 19729-19737.
(28) Sawai, D.; Tsugane, Y.; Tamada, M.; Kanamoto, T.; Sungil, M.; Hyon, S.-H. Crystal Density and Heat of Fusion for a Stereo-Complex of Poly(L-Lactic Acid) and Poly(D-Lactic Acid). *J. Polym. Sci. Part B: Polym. Phys.* **2007,** *45*, 2632-2639.
(29) Loomis, G. L. Polylactide Stereocomplexes. *Polym. Prepr. (Am. Chem. Soc. Div. Polym. Chem.)* **1990,** *31*, 55.
(30) Fujita, M.; Doi, Y. Annealing and Melting Behavior of Poly(L-Lactic Acid) Single Crystals as Revealed by in Situ Atomic Force Microscopy. *Biomacromolecules* **2003,** *4*, 1301-1307.
(31) Fischer, E. W.; Sterzel, H. J.; Wegner, G. Investigation of the Structure of Solution Grown Crystals of Lactide Copolymers by Means of Chemical Reactions. *Kolloid-Z.u.Z.Polymere* **1973,** *251*, 980-990.
(32) Pan, P.; Kai, W.; Zhu, B.; Dong, T.; Inoue, Y. Polymorphous Crystallization and Multiple Melting Behavior of Poly(L-Lactide): Molecular Weight Dependence. *Macromolecules* **2007,** *40*, 6898-6905.
(33) Ruan, J.; Huang, H.-Y.; Huang, Y.-F.; Lin, C.; Thierry, A.; Lotz, B.; Su, A.-C. Thickening-Induced Faceting Habit Change in Solution-Grown Poly(L-Lactic Acid) Crystals. *Macromolecules* **2010,** *43*, 2382-2388.
(34) Okihara, T.; Tsuji, M.; Kawaguchi, A.; Katayama, K.; Tsuji, H.; Hyon, S. H.; Ikada, Y. Crystal Structure of Stereocomplex of Poly(L-Lactide) and Poly(D-Lactide). *J. Macromol. Sci. Part B: Phys.* **1991,** *B30*, 119-140.
(35) Hoogsteen, W.; Postema, A. R.; Pennings, A. J.; Ten Brinke, G.; Zugenmaier, P. Crystal Structure, Conformation and Morphology of Solution-Spun Poly(L-Lactide) Fibers. *Macromolecules* **1990,** *23*, 634-642.

For Table of Content Use Only

Structure and Morphology of Poly(lactic acid) Stereocomplex Nanofiber Shish Kebab

Qing Xie, Xiaohua Chang, Qian Qian, Pengju Pan, Christopher Y. Li